Mapping the thickness of slush on sea ice with multi-frequency EM induction sounding

Neudert, Mara; Briggs, Robert; Bell, Trevor; Hendricks, Stefan; Haas, Christian

Publisher's version / Version de l'éditeur:

https://doi.org/10.1016/j.coldregions.2025.104767

Cold Regions Science and Technology, 243, C, pp. 1-15, 2025-11-24

Cold Regions Science and Technology 243 (2026) 104767

Contents lists available at ScienceDirect

Cold Regions Science and Technology

journal homepage: www.elsevier.com/locate/coldregions

Mapping the thickness of slush on sea ice with multi-frequency EM induction sounding

Mara Neudert [a,*], Robert Briggs [b], Trevor Bell [c], Stefan Hendricks [a], Christian Haas [a,d]

[a] Alfred Wegener Institute, Am Handelshafen 12, 27570 Bremerhaven, Germany
[b] National Research Council Canada, Oceans, Coastal and River Engineering Research Centre, St. John's, A1B 3T5, Newfoundland and Labrador, Canada
[c] Department of Geography, Memorial University of Newfoundland, St. John's, A1B 3X9, Newfoundland and Labrador, Canada
[d] Institute of Environmental Physics, University of Bremen, Otto-Hahn-Allee 1, 28359 Bremen, Germany

ARTICLE INFO

Keywords:
Arctic sea ice
Slush thickness measurement
Multi-frequency EM induction sounding
Snow ice

ABSTRACT

Slush from flooding of sea ice contributes significantly to the sea ice mass balance in the Arctic and Antarctic and poses significant hazards for Arctic communities, affecting the safe use of sea ice for travel, hunting, and other activities. This study demonstrates the effectiveness of multi-frequency electromagnetic (EM) induction sounding for the joint retrieval of slush and ice thicknesses. For the multi-frequency GEM-2 instrument, we identified optimal frequency combinations, for example 5, 10, 20, 30, and 93 kHz, through inversion of synthetic data with realistic noise to achieve minimal mean absolute errors (MAE) of less than 5 cm for slush as thick as 60 cm.

Field EM surveys, validated with coincident drill hole data, demonstrated reliable performance of the method under practical field conditions for slush layers up to 20 cm thick. Instrument calibration was robust but faced challenges at sites where snow and ice conditions deviated from the ideal one-layer model for snow and ice. The inclusion of varying sea ice conductivities in the calibration process enhanced reliability, and we show that a single instrument calibration remains stable for over a week for this instrument of the newest GEM-2 generation.

The method's transferability to airborne applications, such as drone-mounted surveys, offers the potential to eliminate operator risks associated with ground-based measurements on thin ice with thick slush. Overall, multi-frequency EM induction sounding provides a time-efficient and accurate tool for mapping the separate thicknesses of slush and of snow-plus-ice thicknesses.

1. Introduction

Under conditions when ice is relatively thin and snow accumulation is high, the snow's weight may be sufficient to depress the snow-ice interface below the sea surface. This allows seawater to infiltrate the snow, forming a slush layer. Slush can later freeze into a salty, granular ice layer called snow ice (Jeffries et al., 2001). This process makes a significant contribution to sea ice mass balance. Snow ice constitutes approximately 7%–40% of Antarctic sea ice, varying by region and season. It makes up about 10% of ice in the Weddell Sea (Lange et al., 1990) and up to 40% in the Bellingshausen and Amundsen seas (Jeffries et al., 2001).

For Arctic communities, thick slush poses severe risks for travel on sea ice because snowmobiles and sleds can get stuck. Slush is undetectable to the driver because it forms at the snow-ice interface beneath an intact layer of snow. Recent trends in Arctic weather and climate suggest increasingly dangerous sea ice travel conditions, especially on traditional trails that developed under past climate conditions (Bell et al., 2014; Stroeve and Notz, 2018). In the Qikiqtarjuaq region (Fig. 1), our fieldwork location, slush is predominantly observed as a spring phenomenon, occurring when snow thickness increases while ice thickness is either stable or begins to decrease locally. The slush occurrence is typically linked to anomalously thin ice. Ice is thin, typically in regions where polynyas form later in the season (Melling et al., 2015), though this association is not exclusive. For travel safety, local Inuit consider slush hazardous when it exceeds 10–20 cm in thickness, although slush has been reported to reach thicknesses of 40 cm and more (Personal communication, David Iqqaqsaq, 26 April, 2024). No systematic report on the prevalence of slush on landfast sea ice affecting community travel routes is known to the authors. However, an account of slush and its subsequent refreezing into snow

* Corresponding author.
E-mail address: mneudert@awi.de (M. Neudert).

https://doi.org/10.1016/j.coldregions.2025.104767
Received 17 February 2025; Received in revised form 8 September 2025; Accepted 19 November 2025
Available online 24 November 2025

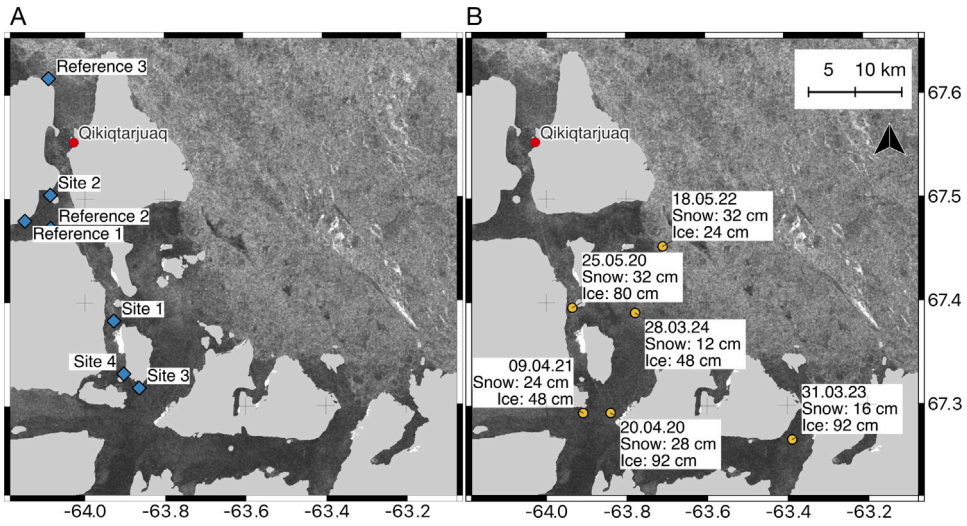

Fig. 1. Map of the region of Qikiqtarjuaq with (A) the sampling locations in 2024, and (B) SmartBUOY deployment locations and their spring snow and sea ice thicknesses 2020–2024 (Data gathered by the SmartICE SmartBUOY program (SmartICE Sea Ice Monitoring and Information Inc, 2021), published with permission). Background is a Sentinel-1 SAR scene from 24 March 2024 (`S1A_EW_GRDM_1SDH_20240324T211958_6CB8_N_1`, retrieved from polarview.aq on 25 March 2024).

ice is documented for Kotzebue (Qikiqtaġruk), Alaska (Mahoney et al., 2021).

Projected changes under the RCP8.5 emission scenario indicate positive trends in mean annual snow water equivalent for the Canadian Arctic in the coming decades (Mohammadzadeh Khani et al., 2022; Bell and Brown, 2018). Additionally, reduced sea ice thickness is projected for the Baffin Island region (Bell and Brown, 2018). There are expected reductions of 27 cm and 26 cm for Clyde River and Iqaluit, respectively, by 2041–2060 compared to the 1970–1989 period (Dumas et al., 2006). These changes suggest an increased potential for slush formation, motivating the search for monitoring tools to ensure the safety of Arctic community travel routes. To map slush as a potential travel hazard, the key target quantities are slush thickness and sea ice thickness. These measurements must be obtained with high spatial resolution along potential travel routes spanning tens to hundreds of kilometers per community. Currently, no dedicated technique exists for monitoring slush and sea ice thickness over larger areas. The primary goal of this study is to assess if the GEM-2 multi-frequency electromagnetic (EM) induction sounding sensor is a suitable instrument for inferring both slush and total thickness, the sum of snow and ice thickness, simultaneously, with a focus on ensuring stability for sea ice travel safety assessments. EM surveys are conducted with the GEM-2, a commercially available EM induction sounding instrument with multi-frequency capabilities, weighing 3.5 kg. It is the only commercial instrument within this weight range, and thus suitable for airborne operations with drones (Vilhelmsen and Døssing, 2022; Karaoulis et al., 2022). The distinctly higher electrical conductivity of saline slush, compared to overlying snow and underlying sea ice, is the relevant physical property for EM induction sounding. Bulk slush electrical conductivity depends on the salinity of the liquid phase of the slush, the connectivity of the liquid phase and it is fraction (or porosity). These properties are expected to vary with the dominant mechanism of infiltration, either lateral by macroscopic flaws or through vertical percolation (Maksym and Jeffries, 2000) and the initial snow density (Provost et al., 2017; Fritsen et al., 2001). When freezing into snow ice, brine drainage reduces slush salinity over time (Maksym and Jeffries, 2001). The role of salt loss and heat exchange in influencing the development and transformation of slush and snow ice following their initial formation remains poorly understood (Maksym and Jeffries, 2001; Saenz and Arrigo, 2012; Jutras et al., 2016). In this study, we neglect these processes leading to a complex vertical salinity profile and adopt a simplified model consisting of a dry snow layer overlying a homogeneous slush layer. To infer slush conductivity, we assume that all pore space in the flooded snow layer is replaced by seawater of the ambient seawater conductivity and temperature. Mixture ratios used in literature are reported to be 1/3 of snow and 2/3 of water based on a snow density of approximately 330 kg/m^3 (Provost et al., 2017), or the liquid phase contributing 62%–65% (Maksym and Jeffries, 2001; Fritsen et al., 2001). By treating slush as a porous medium, with the liquid phase analogous to brine in sea ice (Haas et al., 1997) or the interstitial water in sub-ice platelet layers (Hunkeler et al., 2016b; Haas et al., 2021; Neudert et al., 2024), and applying Archie's law using cementation exponents ranging from 1 to 2, we estimate slush conductivities to range between 1600 and 1050 mS/m (Archie, 1942; Haas et al., 1997) based on a sea water conductivity of about 2500 mS/m in our study region.

To measure sea ice thickness irrespective of slush, EM induction sounding has been widely applied (Haas et al., 1997; Haas, 1998; Reid et al., 2003; Haas et al., 2009, 2021; Itkin et al., 2023) and is routinely used for sea ice safety assessments in Arctic communities through the SmartICE SmartQAMUTIK program (SmartICE Sea Ice Monitoring and Information Inc, 2021). Specifically, this method infers total thickness, defined as the distance from the top of the snow to the sea ice–sea water interface, or the sum of the thicknesses of snow and ice. Due to the low conductivity contrast between sea ice (50 mS/m) and snow (0 mS/m) that is difficult to resolve electromagnetically, the two media are treated as a single-layer medium with negligible electrical conductivity compared to seawater (e.g., 2550 mS/m in the winter Arctic Ocean) (Reid et al., 2006; Haas et al., 2008, 1997). The EM response is a function of the distance of the sensor to the sea ice–sea water interface, which allows for the inference of total thickness.

The higher electrical conductivity of slush, compared to surrounding sea ice and snow, can be leveraged to simultaneously infer slush thickness alongside total thickness in multi-frequency EM induction sounding. When accounting for an additional slush layer, the standard single-layer subsurface model is expanded into a three-layer model of snow, slush, and ice. To resolve the thicknesses of three layers and the slush conductivity, with known and fixed conductivities for sea ice, snow, and sea water, EM data acquisition and inversion must be done with multiple frequencies, each providing different depth sensitivity (Hunkeler et al., 2015, 2016a,b; Neudert et al., 2024). In this study, inversion is performed using the API framework of EMagPy (McLachlan et al., 2021) to identify the three-layer subsurface model that best

fits to measured inphase and quadrature responses at the respective frequencies.

In the first part of this study, we use a forward model to generate synthetic EM responses for subsurface models with layer thickness combinations that satisfy isostatic conditions, i.e., the slush depth is determined by the freeboard according to Mahoney et al. (2021). The choices for modeled layer thicknesses are guided by typical spring sea ice and snow thicknesses on Arctic landfast ice (Fig. 1B) and in the Weddell Sea (Arndt et al., 2021), spanning a broad range of ice thicknesses from 24 cm for thin ice around Qikiqtarjuaq to the modal thickness of about 250 cm from second-year ice in the Weddell Sea, and snow depths ranging from 0 cm to 80 cm. We used a constant conductivities of 0 mS/m for snow, 1600 mS/m for slush, 50 mS/m for sea ice, and 2520 mS/m for sea water. We invert the synthetic data and analyze the sensitivity of the results to frequency selection and instrumental noise, as well as the accuracy achievable in simultaneously resolving slush and total thickness.

In the second part of this study, we transferred the methods used for synthetic data inversion to real EM surveys conducted at seven different sites in the Qikiqtarjuaq region in spring 2024. EM slush and total thicknesses were validated against manual measurements taken from drill holes and snow pits co-located with EM surveys along several 250-m-long transects. In addition to surveys along these transects, larger-scale mapping was conducted at each site to study the spatial slush and thickness distributions.

A key challenge in transitioning from synthetic to field data is the presence of real world sensor drift and offsets, which can vary on a daily basis and must be corrected in calibrations to ensure the reliability of the inversion results (Minsley et al., 2012). Hunkeler et al. (2015) and Neudert et al. (2024) demonstrated that repeated calibrations, similar in approach to those presented by Deszcz-Pan et al. (1998), Reid and Bishop (2004), Brodie and Sambridge (2006) and Minsley et al. (2012), are both effective and necessary to accurately invert multi-frequency EM measurements for subsurface layer thicknesses and conductivities. Our calibration data acquisition procedure follows the common practice to acquire EM data at multiple instrument heights over a simple target of level sea ice with known thickness on a daily basis (Hunkeler et al., 2015; Itkin et al., 2023). This study is the first to simultaneously invert for relatively thin slush and total thicknesses, and we anticipate that our calibrations will require high accuracy, thus we set an error criterion to assess whether a calibration is sufficiently accurate. Additionally, as this is the first study using the latest GEM-2 generation (700 series), we expect improved performance and stability over time. We test whether daily calibration is necessary, or if a single calibration during a two-week field period would suffice.

2. Materials and methods

The environmental conditions influencing slush formation and the EM instrumentation are first described, establishing the boundary conditions for the generation of synthetic data. Forward models of EM responses are then generated for various plausible combinations of snow, ice, and slush thicknesses and are inverted to evaluate the expected accuracy of the method under field conditions to guide the selection of optimal frequencies and to quantify the impact of noise on measurement accuracy. The field data collection and calibration procedures are presented, followed by a thorough description of our calibration approach and an assessment of the quality of each calibration.

2.1. Slush geophysical properties

2.1.1. Slush thickness

Slush can form when the sea ice freeboard is negative. For a given sea ice and snow mass in isostatic equilibrium, the sea ice freeboard follows from Archimedes' principle of buoyancy. The slush thickness will correspond to he negative freeboard value according to the equation given by Mahoney et al. (2021) for the ice freeboard F_i

$$F_i = \frac{1}{1 - v_l d_f}\left(H_i - \frac{\rho_i H_i + \rho_{sn} H_{sn}}{\rho_w}\right), F_i < 0 \quad (1)$$

where is ρ_w is the density of water, ρ_i is the density of ice, ρ_{sn} is the density of snow, H_i is the thickness of the ice, and H_{sn} is the thickness of the snow. We use typical densities of 320 kg/m^3 for Arctic snow (King et al., 2020), 920 kg/m^3 for sea ice (Timco and Weeks, 2010), and 1024 kg/m^3 for sea water. d_f represents the fraction of the negative freeboard depth that floods. Following Mahoney et al.'s (2021) assumption, we estimate this fraction to be about 1, suggesting that seawater has an efficient pathway to the ice surface. v_l is the volume fraction of the flooded snow that is occupied by liquid water. We use a volume fraction of liquid water of 65% (Fritsen et al., 2001), implying an average ice volume of 35% in the slush layers. The magnitude of the negative freeboard can exceed twice the value estimated using the standard equation for freeboard, which would be Eq. (1) without the first term. This first term accounts for the fact that flooded snow displaces a fraction of its volume, thereby reducing the upward buoyancy force (Mahoney et al., 2021).

2.1.2. Slush, sea ice and sea water conductivity

With the assumption that slush is composed of 35% ice with negligible electrical conductivity and 65% sea water with a conductivity of 2520 mS/m, we calculate the bulk slush electrical conductivity using Archie's Law to convert porosity Φ and liquid conductivity of σ_l to electrical conductivity σ_{slush} according to $\sigma_{slush} = \sigma_l \Phi^m$ (Archie, 1942; Haas et al., 1997). A cementation factor m is a measure of the pore space connectivity. A cementation factor of 2.0 gives a lower limit of 1056 mS/m to the slush conductivity, while a cementation factor of 1.0, equivalent to the parallel model (simply the arithmetic mean of the conductivities of liquid and solid phase), suggests an upper conductivity limit of 1625 mS/m. For the forward models in this study, we assume a slush conductivity close to the upper limit of 1600 mS/m, a sea water conductivity of 2520 mS/m, and a sea ice conductivity of 50 mS/m (Haas et al., 1997). The upper limit is used because, unlike congelation and granular sea ice, all the pores in slush are well connected (Maksym and Jeffries, 2000).

2.2. EM (GEM-2) sensor parameters, forward modeling and inversion

Here we used the newest GEM-2 (700 series) instrument generation. The GEM-2 is a frequency-domain induction sensor operated in horizontal-coplanar mode and covers a frequency range of 1–93 kHz, up to 10 discrete frequencies can be selected simultaneously. The receiver–transmitter spacing is 1.670 m and the bucking coil-transmitter spacing is 1.035 m (GEM-2 700er series). An external GPS antenna provides positions with 3 m accuracy. The instrument returns the ratio of secondary to primary EM field as inphase (real component) and quadrature (imaginary component) in parts per million (ppm) for each frequency with a sampling rate of 10 Hz.

The equations for the EM response to a vertical dipole over a layered earth are given for instance by Wait (1982) and we use the implementation by McLachlan et al. (2021) in the EMagPy advanced programming interface for forward modeling and inversion of EM data, which was also used by Neudert et al. (2024). In EMagPy the inverse problem can be solved by a number of optimization methods from the SciPy package (Virtanen et al., 2020).

Forward model and inversion schemes for data from the GEM-2, operated in highly conductive environments, must account for a nonlinear signal bias introduced by the instrument's passive bucking coil, which we accounted for Hunkeler et al. (2016a) and Neudert et al. (2024).

Based on typical spring sea ice and snow thicknesses on Arctic landfast ice and typical thicknesses in the Weddell Sea (Arndt et al.,

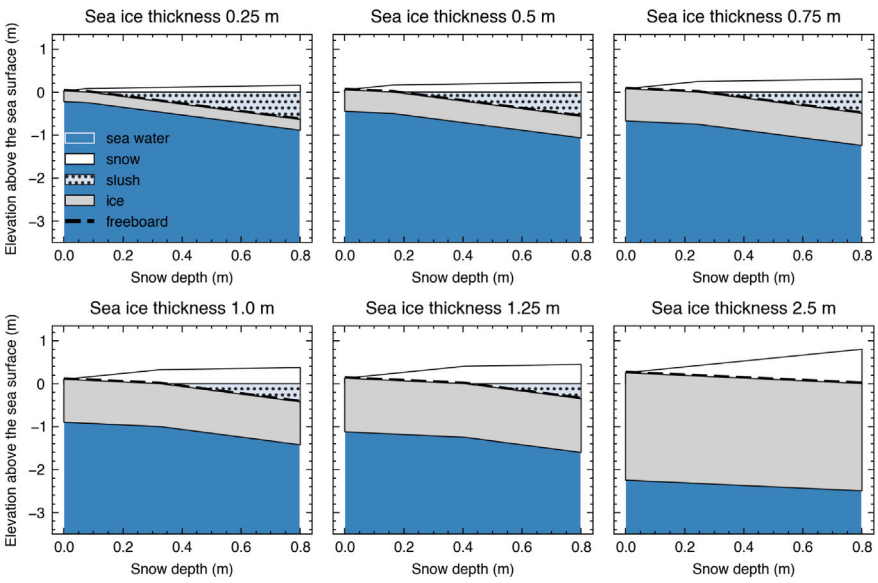

Fig. 2. Models of the subsurface used to generate synthetic data. Each panel shows one model, where the ice thickness was kept constant while snow thickness was increased (from left to right), and slush thickness was calculated according to Eq. (1).

2021) we set up six forward models with fixed ice thicknesses of 0.25, 0.50, 0.75, 1.00, and 1.25 m, and to ensure that we can resolve thicker ice we include a model with 2.5 m ice thickness (Fig. 2). For a given ice thickness, we let snow thicknesses increase from 0 to 0.80 m in increments of 5 mm and compute slush thickness based on Eq. (1) with the parameters stated above. As a result, our models cover slush thicknesses between 0–0.64 m. The mean slush and mean total thickness across all model data points is 0.15 m and 1.44 m, respectively. These mean thickness are 0.24 m and 1.28 m if we only take into account model data points where slush is present.

Fig. 3 presents the inphase and quadrature responses to models incorporating a slush layer over 0.5 m and 1.0 m sea ice thickness (see Fig. 2), relative to the responses to models where the slush layer is replaced with an equivalent thickness of snow (conductivity of 0 mS/m). Except at the highest frequency and for thin ice (up to 0.75 m), the presence of slush of any thickness increases the EM response across all frequencies, compared to the model without slush. The magnitude of this change depends on the thickness of the underlying sea ice. For thin ice below 1.0 m, lower frequencies demonstrate greater sensitivity compared to higher frequencies. For instance, the presence of a 10 cm thick slush layer on 50 cm thick ice alters the inphase by 22% at 5 Hz and by −8% at 93 kHz (Fig. 2A). As the ice gets thicker, the lower frequencies get less sensitive, the changes in inphase signal caused by a 10 cm thick slush layer on 100 cm thick ice are 14% at 5 kHz and 24% at 93 kHz (Fig. 2B). This percentage change represents the change relative to the signal in the model without slush.

Before inversion, random (Gaussian) noise of 60 ppm is added to all responses, representing the mean of observed random instrument noise (Table A.2 and Neudert et al., 2024). We use the same inversion set up for inversion of synthetic data and field data. For detailed implementation, refer to the appendix (Table A.6).

The inversion results yield the depths of the layer interfaces, specifically: (1) the distance from the snow surface to the snow-slush interface, (2) the distance from the snow surface to the slush-sea ice interface, and (3) the distance from the snow surface to the sea ice-seawater interface. From these results, we derive the slush thickness, calculated as the difference between the snow-slush and slush-sea ice interface depths, and the total thickness, measured as the distance from the snow surface to the sea ice-sea water interface. This approach is necessary due to the challenges in resolving the snow-sea ice interface, caused by the low conductivity contrast between these media.

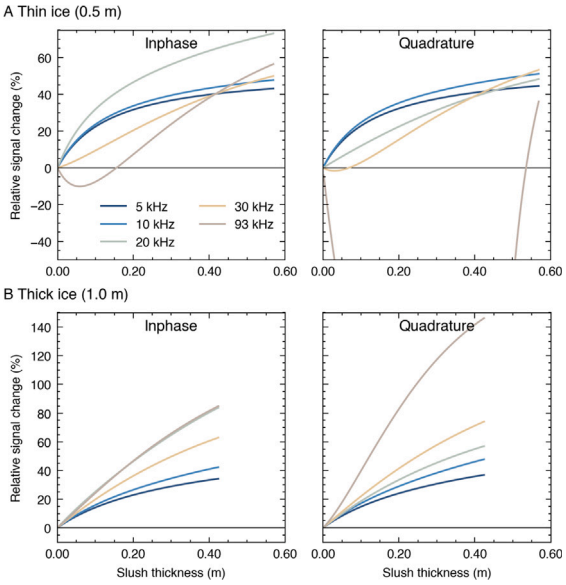

Fig. 3. (A) and (B) each show inphase (left) and quadrature (right) signal changes for five frequencies (5, 10, 20, 30 and 93 kHz). For each component, the relative signal change is determined by computing the difference between the response of a model with slush and a model without slush (but with identical snow and ice thicknesses) and normalizing it by the absolute response of the model without slush. The subsurface models used to generate these data are shown in Fig. 2.

Our model study highlights that, in the presence of slush, accurately resolving the interface positions still remains more challenging than determining the slush and total thickness.

2.3. Optimization of frequency combinations and assessment of noise influence

Using the synthetic data, we evaluate 12 arbitrary frequency combinations to identify the optimal configuration. This is achieved by calculating the mean absolute error (MAE) for both slush thickness and

total thickness across all inverted subsurface model data points for each frequency combination.

For the frequency combination of 5, 10, 20, 30, and 93 kHz, we evaluated how different levels of random noise in the EM data influence inversion outcomes. This analysis is crucial as field tests indicate that stationary GEM-2 instruments experience average noise levels ranging from 35 to 154 ppm (Table A.2). However, noise levels are expected to increase due to instrument movement when towing the instrument on a sled (Neudert et al., 2024). To simulate these effects, forward models were generated with eight noise levels (0, 50, 100, 150, 200, 250, 300, and 600 ppm). For each noise level, the average MAE across all model data points of the inverted slush thickness and total thickness is used for a systematic assessment of noise impact on inversion accuracy.

All modeling scenarios and all co-located manual and EM slush thickness retrievals that were not able to obtain slush and total thickness within an accuracy of 10 cm where flagged unsuitable (outliers). This is based on our assumption that an accuracy of ±10 cm or better is needed to gather reliable data for travel safety assessment. For our EM slush distribution mapping surveys, no coincident manual validation data exist, thus we deviate from this definition of outliers. Instead, we consider all EM slush thicknesses of 20 cm and more as outliers, as slush exceeding this thickness was practically never observed at any site.

2.4. Field data

From 27 April to 6 May 2024 in Qikiqtarjuaq, Nunavut, Canada, we targeted sites that were diverse in slush layer properties and conducted EM surveys co-located with manual thickness measurements to characterize the extent and nature of the slush zones (Fig. 1A). In addition, we sampled three sites without slush, which we call Reference sites. Slush was generally not omnipresent and not as deep as reported by local Inuit at other times. Upon arrival at a site, we laid out a sampling cross with 250 m side length, approximately oriented along the cardinal directions, for EM surveys and co-located thickness drill holes and manual slush thickness measurements every 25 m along the two axes. To capture the extent of the slush zones and larger-scale spatial variability, the area was mapped with the GEM-2, usually by extending the cross to a square and sometimes adding additional lines. All EM surveys were carried out with the GEM-2 set to the frequencies 5010, 9990, 20 010, 30 030, and 93 090 Hz as this combination was determined optimal in the modeling study. The instrument was mounted on a plastic sled, 18 cm above the snow surface (Fig. 4B).

2.4.1. Comparison of detailed EM transects and co-located validation data

On each 250-m transect, the GEM-2 was towed by two people on both sides of the track using two 6 m long ropes (Fig. 4D) to avoid any disturbance of the slush layer. The team stopped each time the sensor reached a mark for slush sampling and drilling. Stopping at each drilling location ensured the collection of truly coincident data. To maintain precise co-location, flags were placed along the transect to mark drilling sites, ensuring a positional accuracy within 1 m. To preserve the undisturbed slush, all transects were completed before any sampling or drilling activities commenced. Drill holes were spaced 25 m apart at the four sites with slush, as well as during the revisits to these two sites. At the reference sites (which were established as part of fieldwork for drone-towed GEM-2 surveys) drilling was conducted every 10 m.

After the EM surveys, the overlying snow was carefully removed, and sea ice thickness was measured with a thickness gauge through a 5 cm diameter drill hole. Ice freeboard, slush layer, and snow thickness were determined using a ruler. In total, 163 manual slush thickness measurements are available for validation, 131 of which also have an ice thickness measurement. Additionally, at sites 1–4, ice cores were extracted from an area without slush. From the measured temperature and salinity profile in 5 cm steps bulk sea ice conductivities between 47 and 85 mS/m were calculated (Table A.3, Haas et al., 1997).

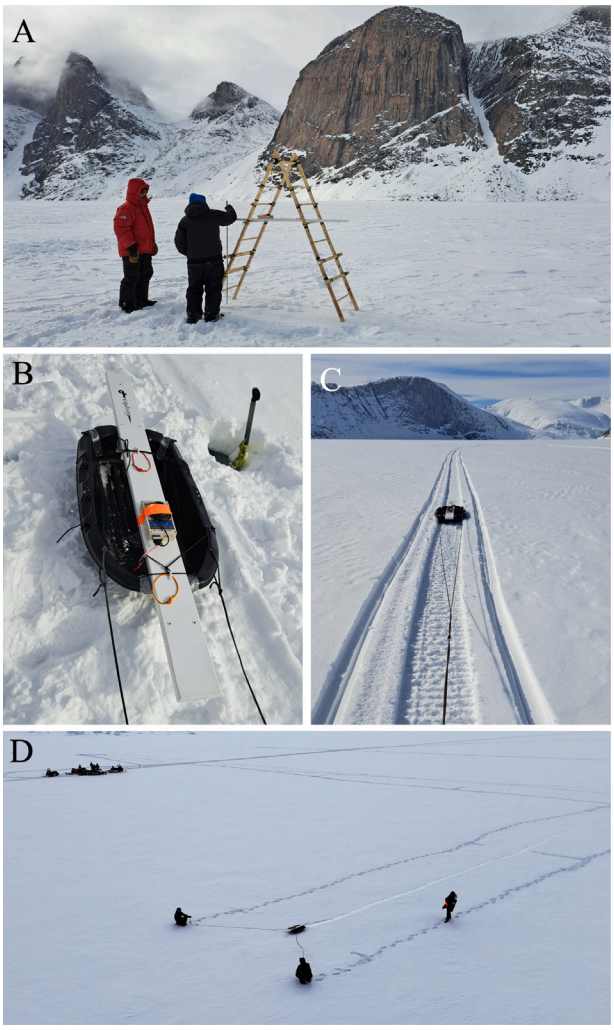

Fig. 4. Photos of (A) a GEM-2 height-step calibration with a wooden ladder, (B) the GEM-2 mounted on the plastic sled, (C) surveying with the GEM-2 towed by the snowmobile, and (D) surveying with two people who tow by hand to avoid disturbance of the snow cover (on the left) while the third person (on the right) is operating the GEM-2 app and placing flags as markers for future drill hole locations.

Before inversion, all EM data measured above a drill hole or slush pit were averaged to obtain representative values. The initial conditions, bounds, and constraints for the inversion are provided in Table A.6, and are identical to those used in the model study with synthetically generated data.

2.4.2. EM slush distribution mapping

To map the distribution of slush within a larger area at each of the four sites with slush, the GEM-2 was towed behind a snowmobile at speeds below 10 km/h using an 8 m long rope (Fig. 4C). At this speed, the sled closely followed the snowmobile's track. The lower surface of the compacted snow in the track caused a downward offset of 4–6 cm of the instrument height, which was accounted for in the inversion by reducing the air layer from 18 cm to 13 cm. In addition, prior to inversion, the data were re-sampled to an equidistant spacing of 1 m. After inversion, a 10-m rolling median filter was applied to the slush thickness results to smooth the data and mitigate the impact of outliers.

2.4.3. Calibration

Previous studies with older GEM-2 sensors highlight the need for daily calibration (Hunkeler et al., 2015; Itkin et al., 2023; Neudert

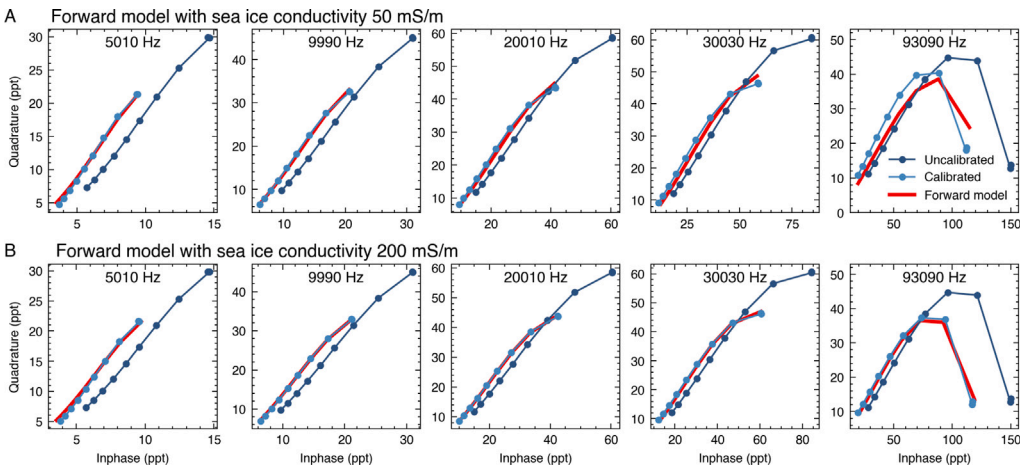

Fig. 5. Calibration on 07 May. Uncalibrated (dark blue) and calibrated (light blue) quadrature versus inphase at different instrument heights above the surface for all five frequencies. Inphase and quadrature decrease with increasing instrument height, from the top right to the bottom left. The graph additionally shows the forward model (red line) (A) with 50 mS/m sea ice conductivity and (B) with 200 mS/m sea ice conductivity. In (A), the mean RMSE across all frequencies is 4.6% (minimum 0.9% for the inphase at 9990 Hz, maximum 21.9% for the quadrature at 93 090 Hz). In (B), the mean RMSE across all frequencies is 1.6% (minimum 0.4% for both, inphase and quadrature, at 20 010 Hz, maximum 4.1% for the quadrature at 93 090 Hz). The forward model with 200 mS/m for sea ice conductivity had the lowest mean RMSE across the frequencies compared to the other models with sea ice conductivities between 0–175 mS/m. The improvement of RMSE compared to the model in (A) with 50 mS/m comes mostly from the improved fit of the two highest frequencies.

et al., 2024). With the 700-series sensors, we assess signal stability and the necessity of daily calibration. Accurate subsurface representation in the forward model remains crucial, especially for thin slush layer inversion.

According to Minsley et al. (2012), three types of calibration coefficients are used to correct for systematic errors that can affect inphase and quadrature recordings due to improper adjustment of the sensor and sensitivity of the sensor electronics to environmental temperatures: (1) zero-level offsets (B_I and B_Q), (2) gain (G), and (3) phase-mixing coefficients (Φ).

In this study, calibration data were collected daily, whenever possible, at a location without slush because the calculation of calibration coefficients requires accurate knowledge of the subsurface structure, needed as input for a forward model of the EM response. However, over slush, these requirements are not met due to the unknown electrical conductivity of the slush layer. The GEM-2 was at ambient temperature. The GEM-2 was elevated step-wise using an 8-step wooden step-ladder (Fig. 4A). Fig. 5 illustrates the change in EM signals (inphase and quadrature) with height. Generally, the signal decreases as the GEM-2 is elevated. Lower inphase and quadrature values, at the bottom left of each panel, correspond to higher positions on the ladder, while higher inphase and quadrature values displayed at the top right of each panel correspond to lower positions on the ladder. The detailed procedure, following Hunkeler et al. (2015), is outlined in Table A.5. Exceptions to this procedure were made at Site 3, where calibration was performed over slush due to the unavailability of a slush-free spot.

After fieldwork, we applied a least squares minimization by comparing the measured EM data with forward model EM data to determine the optimal values B_I, B_Q, G, and Φ. Forward-modeled EM responses are generated for a one-layer surface model, where the single layer corresponds to the mean total thickness measured through drill holes at the calibration site. Below this layer is a homogeneous half-space with seawater conductivity, and above this layer an “air gap” of varying height accounts for different instrument heights. Initially, we set up the forward model with an estimated joint sea ice and snow conductivity of 50 mS/m and a sea water conductivity of 2520 mS/m. To evaluate the goodness of fit for each calibration, we calculated the Root Mean Square Error (RMSE) between the forward model and the calibrated data for each frequency, in percent of the forward response. It became apparent that the highest frequency, assumed to be the most sensitive to sea-ice conductivity due to the lower penetration depth, typically did not yield a good fit with the forward model using 50 mS/m for the sea ice conductivity (see Fig. 5, upper figure, 93 090 Hz quadrature component). Consequently, we varied the sea ice conductivity in the model in increments of 25 mS/m, ranging from 0 to 200 mS/m, and evaluated which conductivity provided the best fit by identifying the lowest average RMSE across all frequencies. The RMSEs and optimal sea ice conductivity for each calibration are summarized in Table A.4.

The inversion results for slush thickness were found to be sensitive to the selected calibration parameters. Using the calibration data from the same day of the survey did not always result in a good agreement between manual slush measurements and EM-derived slush thickness. In a few cases, the failure of a calibration was clearly linked to it being conducted over slush. In other instances, the reasons for high calibration RMSE were less apparent. To justify decisions regarding the reliability of calibrations, we set two criteria: (1) the maximum RMSE for any frequency (inphase or quadrature) must be below 5%, and (2) the optimal sea ice conductivity should fall between 0 and 100 mS/m. Higher conductivities would suggest discrepancies between the real conditions at the calibration site in the forward model assumptions, specifically the assumption of a single-layer snow and ice structure with homogeneously low conductivity. This is supported by the lower average conductivities of 42–85 mS/m from the ice core data.

After discarding calibrations with poor inversion outcomes, fewer than one calibration per day remained. Therefore, we applied a reliable calibration from a date as close as possible to the survey date, resulting in a temporal offset of no more than two days between calibration and survey. To further assess the stability of the GEM-2 over the two-week field campaign, we selected a calibration with a low RMSE from the end of the campaign (Calibration 180 at Site 4, 06 May) and applied it to all EM data. We then evaluated its impact on the inversion results.

3. Results

3.1. Optimization of frequency combinations and assessment of noise influence

3.1.1. Frequency combination

To evaluate the suitability of each frequency combination, the mean absolute error (MAE) of the inverted total thickness and slush thickness across all models is presented in Fig. 6 for each frequency combination. The optimal frequency combination for the study was found to be 5,

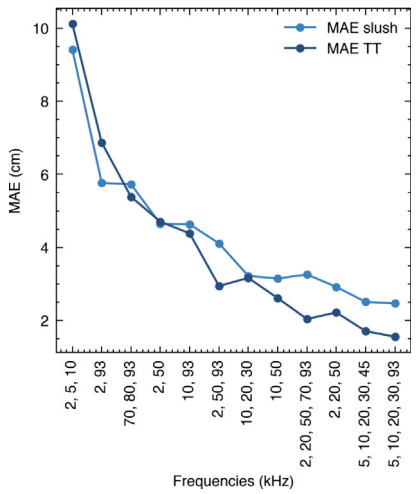

Fig. 6. Mean absolute error (MAE) for inverted slush thickness and total thickness (TT) for the different frequency combinations.

10, 20, 30, and 93 kHz; with a MAE of 2.5 cm for slush thickness and 1.5 cm for total thickness with realistic noise levels and subsurface conditions. Other suitable frequency combinations with similar levels of errors exist, for example 5, 10, 20, 30, and 45 kHz; and 2, 20, and 50 kHz; both have a slush MAE below 3 cm and a total thickness MAE around 2 cm. The resulting error distributions for slush and total thickness using the best frequency combination are slightly narrower compared to those obtained from all frequency combinations applied to the same set of models (Fig. 7).

Next, Fig. 8 shows the inverted layer depths for the optimal frequency combination, the model with the thickest ice thickness (2.5 m) and increasing snow cover (resulting in a maximum total thickness of 3.2 m) showed the highest MAE (4 cm) and the highest number of total thickness outliers, where total thickness was generally underestimated. This is attributed to the greater impact of 60 ppm noise on smaller signal strengths over thick ice. Consequently, the same error in the signal translates to a larger error in total thickness estimation. The models with the thinnest sea ice of 0.25 m and 0.50 m have the highest MAE of 5 cm for slush.

Furthermore, it is evident from Fig. 8 that although slush thickness can be accurately resolved, the positions of the slush-snow interface and the slush-sea ice interface may not be correctly identified, at least not for thin slush or in the absence of slush. Thus, providing separate snow and ice thickness measurements from EM remains impractical, and reliance on total thickness measurements is still necessary.

3.1.2. Noise

The slush and total thickness MAE increases almost linearly with increasing noise in Fig. 9. However, when increasing the modeled noise to 600 ppm, which is well above the observed standard deviations for stationary GEM-2 measurements, which range from 35 ppm for quadrature at 5010 Hz to 154 ppm for inphase at 93 090 Hz (Table A.2), the MAE for slush and TT does not exceed 6 cm. This allows for some tolerance to noise that may arise during actual surveys, caused by the motion of the sled carrying the sensor. Fig. 10 illustrates the effect of different noise levels on inverted thicknesses for a model with 75 cm ice thickness.

The number of outliers increases with the noise level, rising from approximately 2% and 4% for slush and total thickness, respectively, at 0 ppm noise, to 18% and 11% at 600 ppm noise. Outliers were not attributed to significant data misfits (i.e., discrepancies between the inverted inphase and quadrature versus the measured inphase and quadrature) when compared to plausible thickness values. Since there was no correlation between data misfit and thickness errors, the failure to obtain plausible inversion results can only be attributed to an unsatisfactory combination of modeled inphase and quadrature signals at the different frequencies, caused by the random noise.

3.2. Comparison of detailed EM transects and co-located validation data

Having previously examined the results derived from synthetic data generated by a forward model, we now report the outcomes obtained from actual field measurements. The results demonstrate excellent agreement between the GEM-2 method and manual measurements (Figs. 11 and 12). For slush thickness, the EM mean is 4 cm, closely matching the true mean of 2 cm, with a MAE of 4 cm. Similarly, for total thickness, the EM mean of 81 ± 17 cm aligns well with the true mean of 83 ± 17 cm, with a MAE of 4 cm. These results demonstrate the reliability of the GEM-2 for accurately resolving both slush and total thickness, at least within the range of slush thicknesses up to 23 cm encountered in the validation measurements on ice between 55 cm and 151 cm thickness.

The slush conductivity in the starting model of the inversion was 1400 mS/m, and the upper and lower bounds were 1000 and 2520 mS/m, respectively. The average slush conductivity derived from the inversion is 1547 ± 436 mS/m (based on 28 points) for EM slush thicknesses of 5 cm or greater. Similarly, when considering only data with true slush thicknesses of 5 cm or greater, the average conductivity is 1546 ± 448 mS/m (based on 41 points). The initial slush conductivity of the starting model has a significant impact on the final retrieved slush conductivity but does not influence the retrieved thicknesses. This was determined by performing inversions with varying initial slush conductivities between 1000 and 2000 mS/m. The resulting mean conductivity for a starting model value of 1000 mS/m is approximately 1300 mS/m, and the resulting mean conductivity for a starting model value of 2000 mS/m is 1700 mS/m, compared to a mean of about 1500 mS/m when the starting conductivity was 1400 mS/m. True values of slush conductivity are likely highly variable, as some slush was actively refreezing while other slush remained unfrozen, thus we cannot reliably choose the most plausible starting model conductivity and result.

3.3. EM slush distribution mapping

The larger-scale surveys on snowmobile successfully captured plausible spatial patterns of slush and ice thickness at all four sites, the revisits of sites 1 and 2, and the reference sites where no slush was present (Figs. 13 and 14). The small-scale variability is resolved well due to the dense point spacing (1 m) possible due to the measurement rate of 10 Hz. Conducting the surveys was time-efficient compared to manual shoveling and drilling.

At Site 2, slush presence was directly linked to a gradient in total thickness from 70 cm to 35 cm over 250 m, while snow depth remained constant. The observed slush thicknesses are consistent with the thinner ice, which caused negative freeboard under the observed uniform snow load.

Outliers, defined as EM slush thicknesses exceeding 20 cm, make up 2% of the inverted data and are not attributed to large data misfits after inversion compared to surrounding plausible thicknesses, a similar behavior as observed in our model study above (Fig. 8). Applying a moving median over 10 data points (10 m) removed all outliers. The slush conductivities for EM-derived slush thicknesses of 5 cm or more, which is 26% of all data, are comparable to those of 1546 mS/m in the validation data, with a mean value of 1383 ± 314 mS/m.

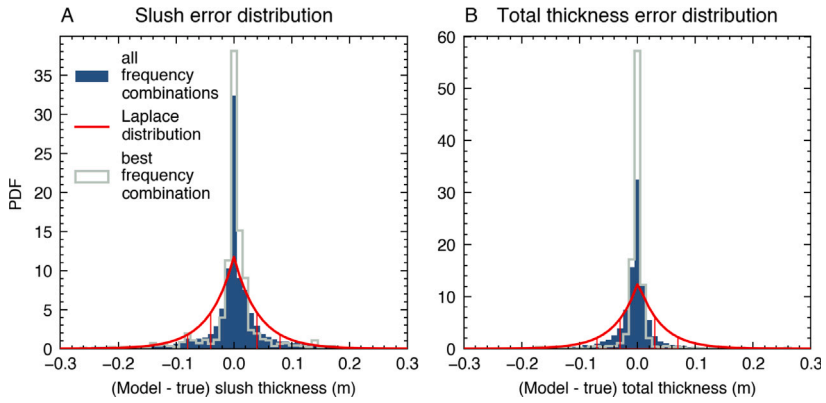

Fig. 7. Error PDF for inverted slush thickness and total thickness for the frequency combination 5, 10, 20, 30 and 93 kHz. The red line is a fitted laplace distribution with the scale factor of the distribution representing the MAE.

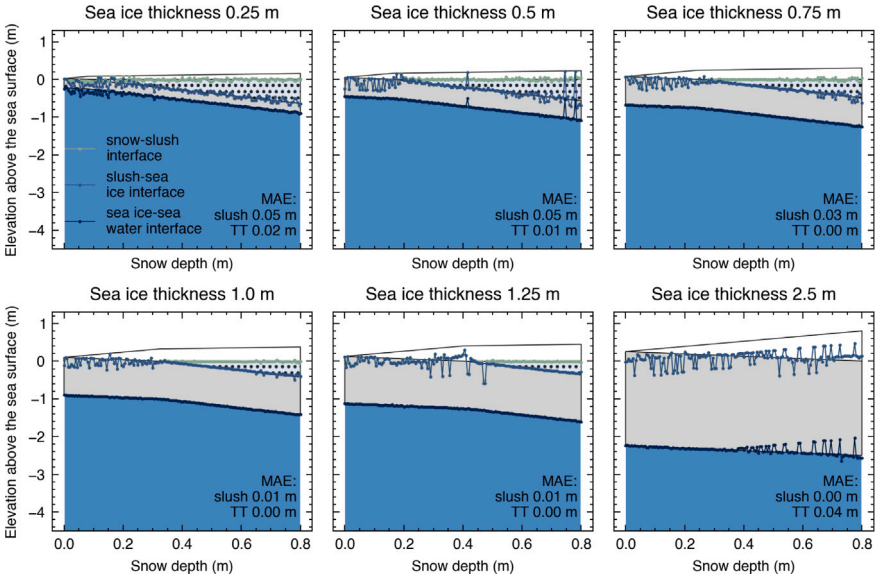

Fig. 8. Inverted slush thickness and total thickness (TT) from synthetic data with 60 ppm Gaussian noise for the optimal frequency combination 5, 10, 20, 30, and 93 kHz.

Table 1
Calibrations utilized in data processing and inversion based on the criteria that the optimal sea ice and snow conductivity must range between 0–100 mS/m, and the maximum RMSE in percent for any frequency (inphase or quadrature) must remain below 5%.

Date	Site	Cal. file nr.	Best conductivity (mS/m)	Used for dates	Remark
2024-04-27	1	106	75	–	No slush, but negative freeboard
2024-04-28	1	115	0	04-27, 04-28, 04-29	
2024-05-01	Ref2	144	0	04-30	
2024-05-01	Ref3	152	50	05-01	
2024-05-04	Test	171	100	05-02,05-03	
2024-05-05	4	174	75	–	Wet snow-ice-interface
2024-05-06	4	180	75	05-05, 05-06, 05-07	

3.4. Calibration

The seven out of 12 calibrations ultimately selected as most reliable according to our criteria of low RMSE and plausible snow and ice conductivity are listed in Table 1. Only five were used, as these resulted in the most accurate EM slush thickness. The two other calibrations (106 and 174) may have been affected by brine infiltration near the surface caused by negative freeboard. One of these calibrations was conducted in a region with widespread flooding but at a specific location that happened to have no slush.

Five calibrations that failed to meet the RMSE threshold of below 5% and a sea ice conductivity of at most 100 mS/m were suboptimally carried out over slush or recently refrozen slush, as no better surface was available nearby. These calibrations yielded models with best-fitting ice conductivities of 125–200 mS/m and high RMSE values at the 93 kHz frequency if a 50 mS/m conductivity model was used (Table A.4). This proves that varying sea ice conductivity in the forward model is a suitable approach to systematically filter out flawed calibrations.

While the choice of calibration location is clearly important, using calibration data from a different day – within a window of up to two days – did not introduce significant errors. Further, using the same

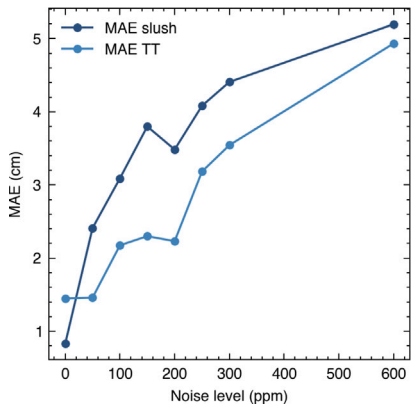

Fig. 9. MAE for inverted slush thickness and total thickness (TT) for different noise levels.

calibration over the entire period also did not result in any significant change of inversion outcomes. This indicates good stability of the new GEM-2 700 sensor under changing temperature and humidity conditions over this time frame.

4. Discussion

Instrument calibration is crucial for retrieving subsurface layer thicknesses and conductivities quantitatively from EM surveys (Minsley et al., 2012; Hunkeler et al., 2015; Neudert et al., 2024). In our study, the height-step calibration approach was applied and found to be a suitable calibration approach. We varied the sea ice conductivity in the forward model from 0 to 200 mS/m and decided that a calibration site was unsuitable when the best-fitting conductivity exceeded 100 mS/m. If the optimal conductivity was between 0 and 100 mS/m, we used the calibration parameters determined at this optimal conductivity. The residual between the forward model and calibrated data was deemed satisfactory when below 5%. The cases where this condition was not met corresponded to calibration sites with optimal model conductivity values exceeding 100 mS/m, indicating that the subsurface at these calibration locations did not match the one-layer model assuming homogeneous snow and ice conductivity. Layers with excessively high conductivity within the snow and ice can occur for ice freeboard close to zero, causing brine wicking with a characteristic wet snow-ice interface, which was frequently observed. Further refreezing of slush could have caused layers with distinct conductivity from the surrounding snow and ice. These circumstances are difficult to avoid before selecting a calibration spot, as assessing the conditions would require removing snow over a large area, which is time-consuming.

Applying calibration parameters from a different day than the actual survey, or even using the same calibration parameters over the entire two-week field period, resulted in accurate retrievals of slush and total thickness. This implies that the GEM-2 could potentially be used as a real-time detector for slush. To our knowledge, this is the first dataset of sea ice surveys and calibrations using the newer generation of the GEM-2 sensor (700 series), as opposed to the 400 and 500 series used in previous studies. Ideally, using the same calibration throughout an entire season would improve the robustness and efficiency of the method. The daily mean temperatures during our survey period ranged from −15 to −5 °C (Government of Canada, 2024), which does not cover the full range of temperatures expected throughout the sea ice season. Further evaluation of the long-term reliability of instrument calibration over extended periods would be beneficial.

The range of slush thicknesses examined in this study is crucial for assessing the applicability of GEM-2 retrievals under various conditions, particularly when slush poses a travel hazard. In our field data, the slush thicknesses encountered were generally below 20 cm and were not widespread, thus not posing a significant travel hazard. Based on this field data, we observed a mean absolute error (MAE) of 4 cm when comparing slush thickness measurements from EM and manual data (Fig. 11), which is consistent with the error observed in the synthetic study (Fig. 6). This comparison suggests that the GEM-2 method performs well within the slush thickness range represented by both datasets. Furthermore, the agreement between the synthetic models and field data implies that the GEM-2 method is also effective for estimating thicker slush layers, as demonstrated in the model study, which successfully accounted for slush thicknesses up to approximately 60 cm. Therefore, the GEM-2 method is anticipated to be a valuable tool for monitoring thicker slush as a potential travel hazard. However, surveying with a snowmobile is impractical in this case due to the risk of becoming immobilized in deep slush. Using a drone-towed EM sensor could offer significant benefits. Vilhelmsen and Døssing (2022) and Karaoulis et al. (2022) have demonstrated the feasibility of geological surveys using a drone-towed GEM-2, provided the separation between the drone and the GEM-2 is sufficiently large to mitigate electronic noise in the EM data. However, numerous technical and logistical challenges must still be addressed before it can be operationalized.

A limitation of this study is the lack of data to validate the EM-derived slush conductivity against measured slush conductivities. Slush conductivity can fluctuate significantly based on environmental factors such as initial snow density, temperature, and the freezing or melting state (Maksym and Jeffries, 2000, 2001). In the inversion, slush conductivity is treated as a free parameter, with resulting values spanning the full permissible range of 1000–2500 mS/m and mean values typically ranging between 1300–1500 mS/m. In the slush distribution mapping surveys, only 26% of the data resulted in inverted slush thicknesses of 5 cm or more, and just 3% exceeded 10 cm. Such thin slush is at the limit of where slush conductivity variations can be accurately resolved through inversion. In addition, the inverted slush conductivities and their variability may not represent true slush conductivity variations but could instead be influenced by vertical conductivity gradients within the sea ice. Sites 3 and 4, along with the revisit of Site 1, exhibited more complex snow, slush and ice profiles in the pit and drill hole data, where slush was actively refreezing. For example, Site 3 had a hard snow-ice layer on top of very liquid slush. At other sites, partial snow-ice layers were present. The field work plan was not specifically designed to study these effects in detail or their influence on EM slush thickness retrieval. Consequently, the challenge of reliably retrieving slush conductivity using EM induction sounding remains an open area for further investigation.

Outliers in the inverted data are a common challenge in geophysical inversion and also affected our results, particularly with increasing noise levels in the synthetic data. In the field data, outliers were generally rare, with less than 2% showing implausible slush thicknesses exceeding 20 cm which was not observed in the manual validation data. The percentage of outliers in the model study with synthetic noise of 60 ppm matches those in the inverted field data. The outliers did not correspond to large data misfits, as no significant discrepancies were found between the inverted inphase and quadrature and the measured inphase and quadrature. Instead, these outliers are attributed to noise or local deviations from the idealized 3-layer subsurface model. The application of a 10-meter rolling median window as a smoothing technique, helped to reduce the number of these outliers.

5. Conclusions

This study demonstrates the effectiveness of the GEM-2 sensor for simultaneously measuring slush and total thickness on Arctic landfast sea ice. The optimized frequency combination of 5, 10, 20, 30, and 93 kHz yielded the best results in a study using synthetic EM responses to slush thicknesses ranging from 0 to 60 cm over ice thicknesses

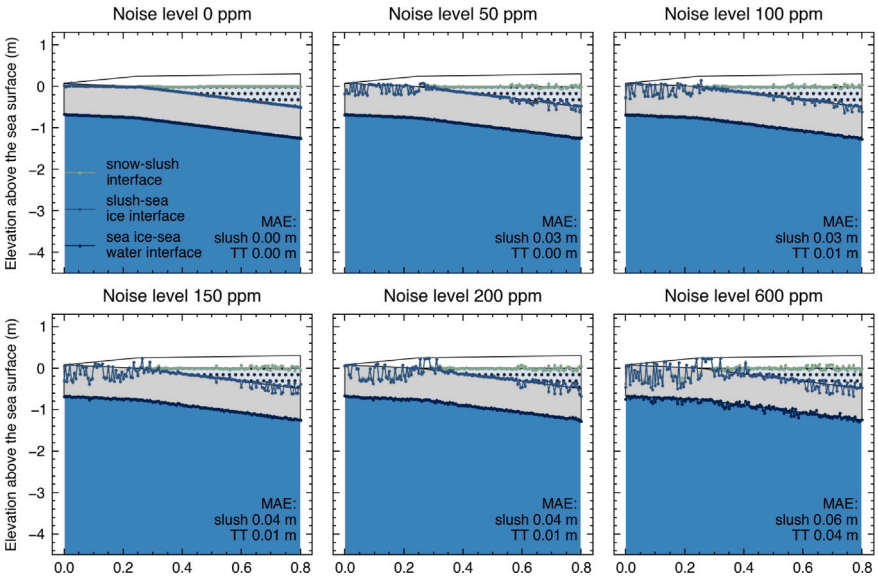

Fig. 10. Inverted slush thickness and total thickness (TT) from synthetic data of 75 cm ice thickness and increasing levels of Gaussian noise (0, 50, 100, 150, 200, and 600 ppm) for the frequency combination 5, 10, 20, 30, and 93 kHz.

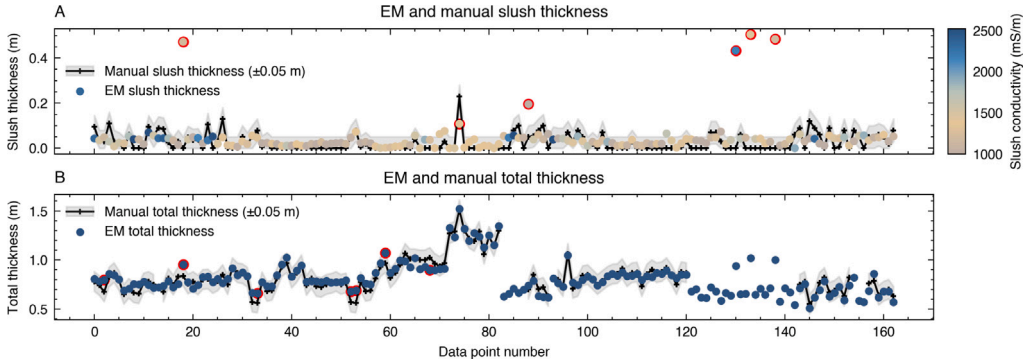

Fig. 11. EM slush thickness and total thickness compared with validation data from drill holes. Markers with a red outline indicate outliers, where the manually measured validation thickness differs by 10 cm or more from the EM thickness. In the upper plot, the color scale represents inverted slush conductivity values associated with the EM slush thickness measurements.

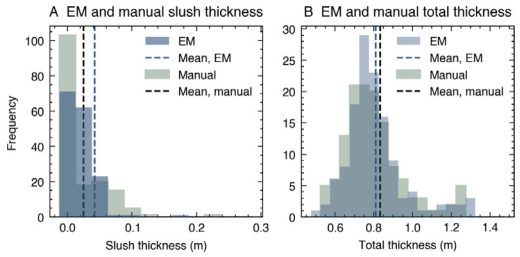

Fig. 12. Histogram of EM slush thickness and total thickness compared with validation data from drill holes. The data presented in this histogram correspond to the same dataset shown in Fig. 11.

between 0.25 m and 2.5 m, achieving mean absolute errors (MAE) of 2.5 cm for slush thickness and 1.5 cm for total thickness. In field surveys, where the average slush thickness was 4 cm and the average ice thickness was 81 cm, the mean absolute error (MAE) between true thicknesses and EM-derived thicknesses was 4 cm for both slush and total thickness. This magnitude of error is consistent with the accuracy observed in the inversion of synthetic data. The infrequent occurrence of slush thicker than 20 cm in our field data, which would be considered a travel hazard, highlights the need for further field studies to explore the performance of the GEM-2 under such conditions.

Part of our EM surveys and manual validation data were collected in areas with refreezing slush, which is expected to cause variations in slush conductivity, potentially influencing the accuracy of slush thickness retrieval. Resolving the slush conductivity or a more complex subsurface conductivity layering, which deviates from our simplified three-layer model (with zero conductivity snow over a homogeneous slush layer with approximately 2/3 seawater conductivity, followed by a homogeneous ice layer), remains an open question. In addition, while our method resolves slush thickness, the identification of the position of the layer interfaces of snow, slush and ice remains challenging. As a result, we continue to use total thickness measurements rather than distinguishing between snow, ice, and slush where present.

Despite the sensitivity of the calibration to sea ice conditions and subsurface heterogeneity, the results demonstrate that the GEM-2 can be calibrated with sufficient accuracy if the calibration site is carefully

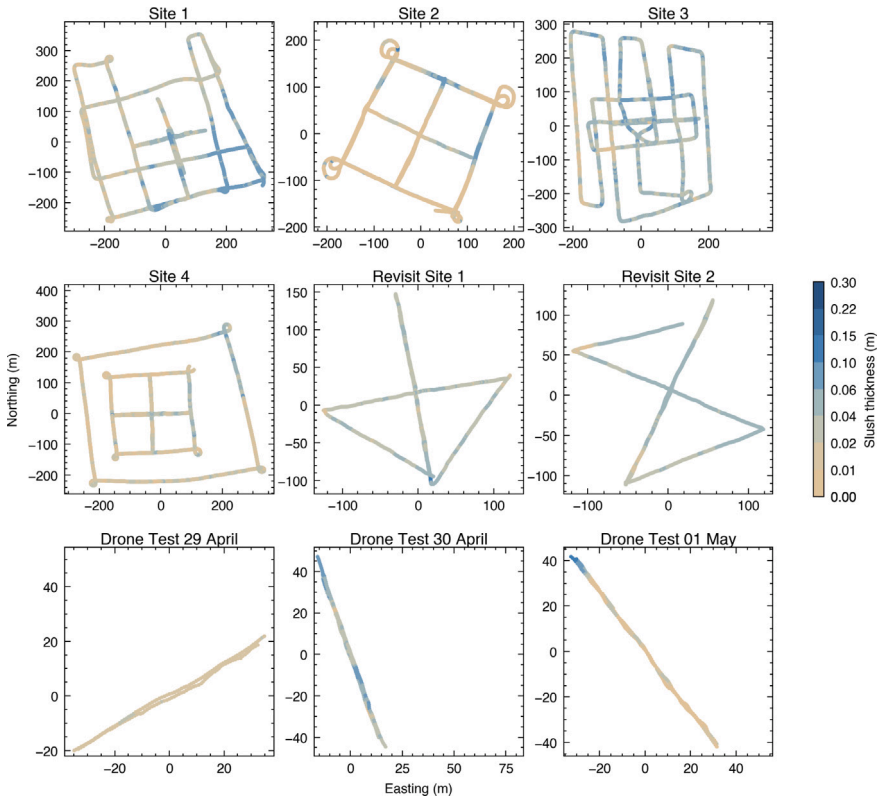

Fig. 13. Maps of EM slush thickness (smoothed with a 10-m rolling median) at the different sites.

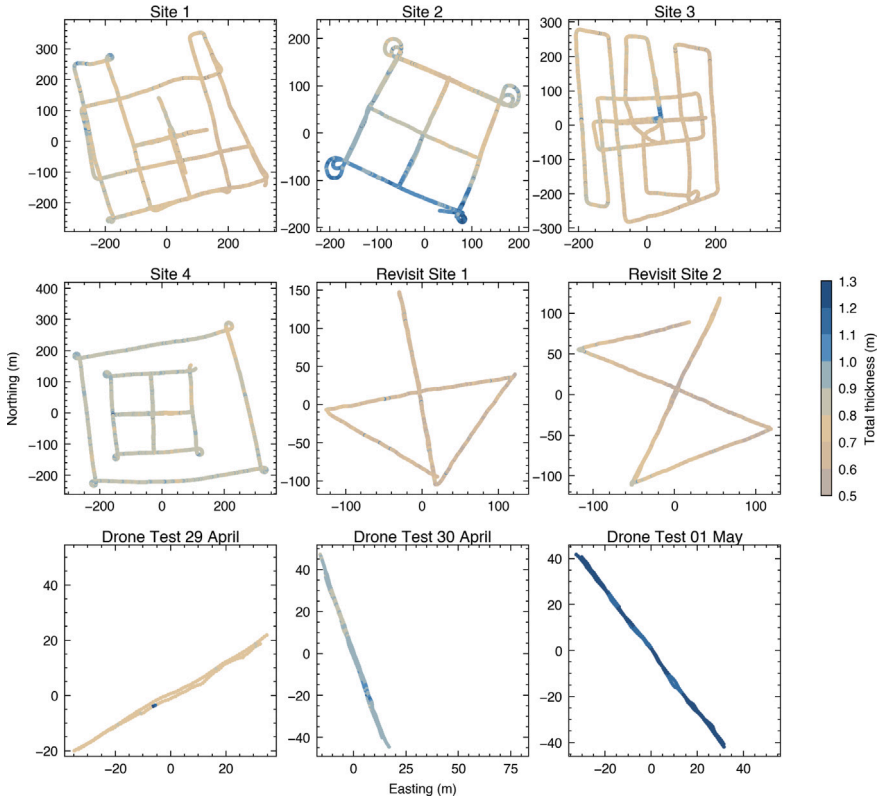

Fig. 14. Same as Fig. 13 but for EM total thickness.

selected. Specifically, areas with higher conductivity within the sea ice and areas with slush should be avoided to ensure accurate calibration. We have developed a method to assess calibration quality and established that, at least for this instrument of the GEM-2 700 series, the calibration remains stable over a two-week period, and daily calibration is not necessary.

Our results validate the GEM-2's potential as a reliable tool for sea ice monitoring, especially for estimating slush and total thickness, where manual measurements are labor-intensive and often impractical. Its portability and low weight make it suitable for integration into drone-mounted systems, offering the potential for broader operational application in community ice condition monitoring (e.g. SmartICE.org), particularly in areas where slush depths prevent safe traverse on snowmobile. Drone-borne GEM-2 surveys could serve as a valuable tool for slush surveying by community operators from a safe distance.

CRediT authorship contribution statement

Mara Neudert: Writing – review & editing, Writing – original draft, Visualization, Software, Methodology, Investigation, Formal analysis, Data curation, Conceptualization. **Robert Briggs:** Writing – review & editing, Supervision, Resources, Project administration. **Trevor Bell:** Writing – review & editing, Supervision, Resources, Project administration, Funding acquisition. **Stefan Hendricks:** Writing – review & editing, Methodology. **Christian Haas:** Writing – review & editing, Supervision.

Funding

Funding for this research was provided by the Canada-Inuit Nunangat-United Kingdom Arctic Research Programme 2021–25, through the Sikuttiaq project.

Declaration of competing interest

The authors declare that they have no known competing financial interests or personal relationships that could have appeared to influence the work reported in this paper.

Acknowledgments

We thank Constanza Salvo, Randy Scharien, Carl Thibault, and David Iqqaqsaq for their invaluable teamwork in the field. A special acknowledgment goes to David Iqqaqsaq, SmartICE Community Operations Coordinator in Qikiqtarjuaq, for his deep local knowledge and his unfailing ability to locate sites with slush, even when its occurrence remained sparse during our time in the area. We acknowledge Anne Irvin's initial fieldwork and tests, which demonstrated the feasibility of slush retrieval with the GEM2. I also extend my gratitude to the SmartICE staff for their support with logistics and travel arrangements.

Appendix A. Sample appendix section

Inversion Settings

See Tables A.2–A.6.

Data availability

Data will be made available on request.

Table A.2
Assessment of instrument noise is carried out using the standard deviations (column "Std") of GEM-2 background signals across different tests conducted in various environmental conditions with the same instrument. The mean values of the signals are also given to illustrate that the instrument noise does not depend on the absolute value of the measured signal.

Site	Site 1		Drone test site 1	
Date	26. Apr		29. Apr	
Duration (s)	302		113	
Frequency	Mean (ppm)	Std (ppm)	Mean (ppm)	Std (ppm)
I, 5010 Hz	13 699	41	13 422	43
Q, 5010 Hz	28 121	35	27 381	44
I, 9990 Hz	28 398	39	27 719	50
Q, 9990 Hz	42 771	39	41 598	48
I, 20 010 Hz	54 492	47	52 984	47
Q, 20 010 Hz	57 249	47	55 669	45
I, 30 030 Hz	75 625	54	73 408	48
Q, 30 030 Hz	61 657	57	60 031	46
I, 93 090 Hz	138 110	154	133 653	86
Q, 93 090 Hz	37 318	129	37 582	85
Mean		64.2		54.2
Site	Parking lot 1		Parking lot 2	
Date	17. Apr		17. Apr	
Duration (s)	115		115	
Frequency	Mean (ppm)	Std (ppm)	Mean (ppm)	Std (ppm)
I, 5010 Hz	4925	55	5327	57
Q, 5010 Hz	−971	50	−911	56
I, 9990 Hz	1945	51	2364	64
Q, 9990 Hz	−1341	47	−1225	64
I, 20 010 Hz	2244	64	2694	90
Q, 20 010 Hz	−1735	61	−1520	87
I, 30 030 Hz	78	65	594	75
Q, 30 030 Hz	−948	60	−635	77
I, 93 090 Hz	−692	94	595	81
Q, 93 090 Hz	−2127	73	−1409	78
Mean		62		72.9
Site	Satellite road 2		Satellite road 3	
Date	20. Apr		20. Apr	
Duration (s)	262		662	
Frequency	Mean (ppm)	Std (ppm)	Mean (ppm)	Std (ppm)
I, 5010 Hz	94	70	441	47
Q, 5010 Hz	99	62	105	49
I, 9990 Hz	236	68	574	48
Q, 9990 Hz	67	60	72	48
I, 20 010 Hz	302	71	606	84
Q, 20 010 Hz	65	64	72	81
I, 30 030 Hz	294	68	550	57
Q, 30 030 Hz	−422	60	−409	58
I, 45 030 Hz	452	64	611	58
Q, 45 030 Hz	−281	56	−311	57
Mean		64.3		58.7

Table A.3
Ice core salinity, temperature, and derived sea ice conductivity data. All data are averaged for the entire sea ice column, with sampling conducted at 5 cm intervals.

Core name	Salinity mean (min–max) (ppt)	Temperature mean (min–max) (°C)	Sea ice conductivity mean (min–max) (mS/m)
S1-C1	3.8 (3.4–4.7)	−2.0 (−2.5 to −1.7)	47 (35–57)
S2-C1	4.0 (3.4–4.9)	−2.1 (−2.4 to −1.7)	50 (35–62)
S3-C1	4.5 (3.1–10.2)	−1.9 (−2.3 to −1.5)	70 (36–230)
S3-C2	5.2 (3.4–11.0)	−2.0 (−2.4 to −1.8)	85 (38–252)
S4-C1	3.7 (3.1–4.4)	−2.2 (−2.7 to −1.7)	42 (29–56)
S1 revisit C1	4.3 (3.0–6.5)	−1.8 (−2.3 to −1.6)	66 (32–137)

Table A.4
Calibration outcomes (goodness of calibration).

Calibration errors for calibration with the best-fitting sea ice conductivity.								
Date	Site	Cal. file nr.	Sea ice conductivity (mS/m)	Mean RMSE (%)	Maximum RMSE (%)	93 090 Hz inphase RMSE (%)	93 090 Hz quadrature RMSE (%)	Remark
2024-04-27	1	106	75	1	2.3	1.1	1.9	[a]
2024-04-28	1	115	0	0.9	2.9	1	2.9	
2024-04-29	Ref1	127	125	1.2	4.8	1.2	4.8	
2024-04-30	Ref2	144	0	1.4	3.5	0.9	3.6	
2024-05-01	Ref3	152	50	1.4	4.2	0.6	3.4	
2024-05-02	3	160	200	2.5	6.2	2.8	6.2	[b]
2024-05-02	3	163	200	2.6	5.1	5.1	4.9	[c]
2024-05-03	3	164	200	5.4	25.4	2.3	25.4	[b]
2024-05-04	Test	171	100	1	3.5	0.9	3.5	
2024-05-05	4	174	75	0.8	1.7	1	1.5	[d]
2024-05-06	4	180	75	0.9	1.8	0.8	1.5	
2024-05-07	1	186	175	1.5	7.8	2.2	7.8	
Calibration errors for calibration with sea ice conductivity set to 50 mS/m.								
Date	Site	Cal. file nr.	Sea ice conductivity (mS/m)	Mean RMSE (%)	Maximum RMSE (%)	93 090 Hz inphase RMSE (%)	93 090 Hz quadrature RMSE (%)	Remark
2024-04-27	1	106	50	1.5	6.4	1.8	6.4	[a]
2024-04-28	1	115	50	1.3	7.1	0.8	7.1	
2024-04-29	Ref1	127	50	1.3	4.5	1.7	4.5	
2024-04-30	Ref2	144	50	1.9	5.7	1.0	2.6	
2024-05-01	Ref3	152	50	1.4	4.2	0.6	3.4	
2024-05-02	3	160	50	5.2	25.6	3.1	25.6	[b]
2024-05-02	3	163	50	4.3	13.9	2.6	13.9	[c]
2024-05-03	3	164	50	8.6	42.2	4.1	42.2	[b]
2024-05-04	Test	171	50	1.5	3.5	1.5	2.4	
2024-05-05	4	174	50	1.5	4.4	1.1	2.5	[d]
2024-05-06	4	180	50	1.3	4.7	1.1	2.6	
2024-05-07	1	186	50	4	21.9	1.2	21.9	

Remarks:
[a] No slush, but negative freeboard.
[b] Slush present.
[c] Slush in the vicinity.
[d] Wet snow-ice interface.

Table A.5
GEM2 height step calibration procedure (ladder calibration).

Nr.	Step	Note
1	Find a level piece of ice without slush.	The less complications, the better. The ideal case is a fully level and completely solid, indicating very low electrical conductivity.
2	Place the ladder on the calibration spot	Snow is not being removed. Ensure the ability to measure the distance of the ice/water interface to the reference surface (top of snow), by not trampling the area.
3	Remove the GEM-2 from the sledge. Place it below the ladder on the surface.	
4	Start GEM-2 data logging, ensure a dedicated file is used for the calibration (Start new SURVEY). Record the file's name in the field book.	It is important that the log for each height step is clean. Everyone should keep a distance of several meters to avoid interference. If erroneous data is recorded, press PAUSE and NEW LINE to generate a new line. Mark line number with invalid data as "invalid" in field notebook.
5	Record that the GEM-2 height is 0.0 cm and that the line number is 1 in field book, log for 20 s. Pause logging.	All heights above the reference surface are measured to the underside of the instrument.
6	Place the GEM-2 on the first ladder step, measure the height from reference surface to instrument underside on both ends of the GEM-2 with a meter stick.	Try to have the GEM-2 as level as possible. The offset between heights on both ends should not be more than 5 cm.
7	Write down the two heights	
8	Press NEW LINE and record for 20 s. The line number displayed now must be recorded.	It is important to record the correct line number associated with the measurements of the specific height step as it will be used to stack all measurements.

(*continued on next page*)

Table A.5 (*continued*).

Nr.	Step	Note
9	Progress to next height step and repeat the procedures.	
10	After reaching the maximum height, repeat the on-surface measurement (height 0)	This is used as a check for instrument drift in the processing.
11	Close survey (optional: shutdown GEM-2).	
12	Remove ladder, drill 5 holes in an X-pattern (one at the center of the ladder position), and 4 at the corners.	
13	Measure the 5 total thicknesses and snow depths and note in field book.	The total thickness refers to the distance between reference surface (here: snow) and sea ice-sea water interface.

Table A.6
Inversion setup and constraints for the geophysical model.

Layer		Fixed	Description
Initial Conditions			
Depth, layer 1	0.222 m	FALSE	Snow depth
Depth, layer 2	0.3456 m	FALSE	Snow plus slush depth
Depth, layer 3	1.666 m	FALSE	Total thickness
Conductivity, layer 1	0 mS/m	TRUE	Snow
Conductivity, layer 2	1400 mS/m	FALSE	Slush
Conductivity, layer 3	50 mS/m	TRUE	Sea ice
Conductivity, layer 4	2520 mS/m	TRUE	Sea water
Bounds			
Depth, layer 1	0.01–1 m	FALSE	Snow depth
Depth, layer 2	0.01–1 m	FALSE	Snow plus slush depth
Depth, layer 3	0.2–4 m	FALSE	Total thickness
Conductivity, layer 1	– mS/m	TRUE	Snow
Conductivity, layer 2	1000–2520 mS/m	FALSE	Slush
Conductivity, layer 3	– mS/m	TRUE	Sea ice
Conductivity, layer 4	– mS/m	TRUE	Sea water
Constraints			
Depth, layer 2 - depth, layer 1	≥0.2 m	–	Inequality constraint, ice thickness must be ≥0.2 m
Regularization and method			
Regularization	L2	–	–
Method	SLSQP	–	–

References

Archie, G.E., 1942. The electrical resistivity log as an aid in determining some reservoir characteristics. Trans. AIME 146 (01), 54–62. http://dx.doi.org/10.2118/942054-G.

Arndt, S., Haas, C., Meyer, H., Peeken, I., Krumpen, T., 2021. Recent observations of superimposed ice and snow ice on sea ice in the northwestern Weddell Sea. Cryosphere 15 (9), 4165–4178. http://dx.doi.org/10.5194/tc-15-4165-2021, URL: https://tc.copernicus.org/articles/15/4165/2021/.

Bell, T., Briggs, R., Bachmayer, R., Li, S., 2014. Augmenting Inuit knowledge for safe sea-ice travel — The SmartICE information system. In: 2014 Oceans - St. John's. pp. 1–9. http://dx.doi.org/10.1109/OCEANS.2014.7003290.

Bell, T., Brown, T.M., 2018. From Science to Policy in the Eastern Canadian Arctic: An Integrated Regional Impact Study (IRIS) of Climate Change and Modernization. ArcticNet, Quebec City.

Brodie, R., Sambridge, M., 2006. A holistic approach to inversion of frequency-domain airborne EM data. Geophysics 71 (6), G301–G312.

Deszcz-Pan, M., Fitterman, D.V., Labson, V.F., 1998. Reduction of inversion errors in helicopter EM data using auxiliary information. Explor. Geophys. 29 (2), 142–146.

Dumas, J.A., Flato, G.M., Brown, R.D., 2006. Future projections of landfast ice thickness and duration in the Canadian arctic. J. Clim. 19 (20), 5175–5189. http://dx.doi.org/10.1175/JCLI3889.1.

Fritsen, C.H., Coale, S.L., Neenan, D.R., Gibson, A.H., Garrison, D.L., 2001. Biomass, production and microhabitat characteristics near the freeboard of ice floes in the Ross Sea, Antarctica, during the Austral Summer. Ann. Glaciol. 33, 280–286. http://dx.doi.org/10.3189/172756401781818653.

Government of Canada, 2024. Daily Data Report for April 2024 - qikiqtarjuaq climate, nunavut, current station operator: Environment and climate change Canada - meteorological service of Canada. https://climate.weather.gc.ca/climate_data/daily_data_e.html?hlyRange=2005-04-20%7C2025-01-15&dlyRange=2005-03-01%7C2025-01-15&mlyRange=2005-04-01%7C2007-11-01&StationID=42803&Prov=NU&urlExtension=_e.html&searchType=stnProx&optLimit=specDate&Month=4&Day=1&StartYear=1840&EndYear=2020&Year=2024&selRowPerPage=25&Line=1&txtRadius=25&optProxType=navLink&txtLatDecDeg=67.546666666667&txtLongDecDeg=-64.031666666667&timeframe=2&time=LST.

Haas, C., 1998. Evaluation of ship-based electromagnetic-inductive thickness measurements of summer sea-ice in the Bellingshausen and Amundsen Seas, Antarctica. Cold Reg. Sci. & Technol. 27 (1), 1–16. http://dx.doi.org/10.1016/S0165-232X(97)00019-0.

Haas, C., Gerland, S., Eicken, H., Miller, H., 1997. Comparison of sea-ice thickness measurements under summer and winter conditions in the Arctic using a small electromagnetic induction device. Geophysics 62, 749–757. http://dx.doi.org/10.1190/1.1444184.

Haas, C., Langhorne, P.J., Rack, W., Leonard, G.H., Brett, G.M., Price, D., Beckers, J.F., Gough, A.J., 2021. Airborne mapping of the sub-ice platelet layer under fast ice in McMurdo Sound, Antarctica. Cryosphere 15 (1), 247–264. http://dx.doi.org/10.5194/tc-15-247-2021.

Haas, C., Lobach, J., Hendricks, S., Rabenstein, L., Pfaffling, A., 2009. Helicopter-borne measurements of sea ice thickness, using a small and lightweight, digital EM system. J. Appl. Geophys. 67 (3), 234–241. http://dx.doi.org/10.1016/j.jappgeo.2008.05.005, Airborne Geophysics.

Haas, C., Nicolaus, M., Willmes, S., Worby, A., Flinspach, D., 2008. Sea ice and snow thickness and physical properties of an ice floe in the western Weddell Sea and their changes during spring warming. Deep. Sea Res. II: Top. Stud. Ocean. 55 (8), 963–974. http://dx.doi.org/10.1016/j.dsr2.2007.12.020.

Hunkeler, P., Hendricks, S., Hoppmann, M., Farquharson, C., Kalscheuer, T., Grab, M., Kaufmann, M.S., Rabenstein, L., Gerdes, R., 2016a. Improved 1D inversions for sea ice thickness and conductivity from electromagnetic induction data: Inclusion of nonlinearities caused by passive bucking. Geophysics 81 (1), WA45–WA58. http://dx.doi.org/10.1190/GEO2015-0130.1.

Hunkeler, P.A., Hendricks, S., Hoppmann, M., Paul, S., Gerdes, R., 2015. Towards an estimation of sub-sea-ice platelet-layer volume with multi-frequency electromagnetic induction sounding. Ann. Glaciol. 56 (69), 137–146. http://dx.doi.org/10.3189/2015AoG69A705.

Hunkeler, P.A., Hoppmann, M., Hendricks, S., Kalscheuer, T., Gerdes, R., 2016b. A glimpse beneath Antarctic sea ice: Platelet layer volume from multifrequency electromagnetic induction sounding. Geophys. Res. Lett. 43 (1), 222–231. http://dx.doi.org/10.1002/2015GL065074.

Itkin, P., Hendricks, S., Webster, M., Albedyll, L., von Arndt, S., Divine, D., Jaggi, M., Oggier, M., Raphael, I., Ricker, R., Rohde, J., Schneebeli, M., Liston, G.E., 2023.

Sea Ice and snow characteristics from Year-Long transects at the MOSAiC Central Observatory. Elementa: Sci. Anthr. 11 (1), 00048. http://dx.doi.org/10.1525/elementa.2022.00048.

Jeffries, M.O., Krouse, H.R., Hurst-Cushing, B., Maksym, T., 2001. Snow-Ice accretion and snow-cover depletion on Antarctic First-Year Sea-Ice floes. Ann. Glaciol. 33, 51–60. http://dx.doi.org/10.3189/172756401781818266.

Jutras, M., Vancoppenolle, M., Lourenço, A., Vivier, F., Carnat, G., Madec, G., Rousset, C., Tison, J.-L., 2016. Thermodynamics of slush and Snow–Ice formation in the Antarctic Sea-Ice zone. Deep. Sea Res. II: Top. Stud. Ocean. 131, 75–83. http://dx.doi.org/10.1016/j.dsr2.2016.03.008.

Karaoulis, M., Ritsema, I., Bremmer, C., De Kleine, M., Oude Essink, G., Ahlrichs, E., 2022. Drone-Borne electromagnetic (DR-EM) surveying in the Netherlands: Lab and field validation results. Remote. Sens. 14 (5335), http://dx.doi.org/10.3390/rs14215335.

King, J., Howell, S., Brady, M., Toose, P., Derksen, C., Haas, C., Beckers, J., 2020. Local-scale variability of snow density on Arctic sea ice. Cryosphere 14 (12), 4323–4339. http://dx.doi.org/10.5194/tc-14-4323-2020.

Lange, A., Schlosser, P., Ackley, S.F., Wadhams, P., Dieckmann, G.S., 1990. 18O concentrations in sea ice of the Weddell Sea, Antarctica. J. Glaciol. 36 (124), 315–323.

Mahoney, A.R., Turner, K.E., Hauser, D.D.W., Laxague, N.J.M., Lindsay, J.M., Whiting, A.V., Witte, C.R., Goodwin, J., Harris, C., Schaeffer, R.J., Sr, R.S., Betcher, S., Subramaniam, A., Zappa, C.J., 2021. Thin ice, deep snow and surface flooding in Kotzebue Sound: Landfast ice mass balance during two anomalously warm winters and implications for marine mammals and subsistence hunting. J. Glaciol. 67 (266), 1013–1027. http://dx.doi.org/10.1017/jog.2021.49.

Maksym, T., Jeffries, M.O., 2000. A One-Dimensional percolation model of flooding and snow ice formation on Antarctic sea ice. J. Geophys. Res.: Ocean. 105 (C11), 26313–26331. http://dx.doi.org/10.1029/2000JC900130.

Maksym, T., Jeffries, M.O., 2001. Phase and compositional evolution of the flooded layer during snow-ice formation on Antarctic sea ice. Ann. Glaciol. 33, 37–44. http://dx.doi.org/10.3189/172756401781818860.

McLachlan, P., Blanchy, G., Binley, A., 2021. EMagPy: Open-source standalone software for processing, forward modeling and inversion of electromagnetic induction data. Comput. Geosci. 146, 104561. http://dx.doi.org/10.1016/j.cageo.2020.104561.

Melling, H., Haas, C., Brossier, E., 2015. Invisible polynyas: Modulation of fast ice thickness by ocean heat flux on the Canadian polar shelf. J. Geophys. Res.: Ocean. 120 (2), 777–795. http://dx.doi.org/10.1002/2014JC010404.

Minsley, B.J., Smith, B.D., Hammack, R., Sams, J.I., Veloski, G., 2012. Calibration and filtering strategies for frequency domain electromagnetic data. J. Appl. Geophys. 80, 56–66. http://dx.doi.org/10.1016/j.jappgeo.2012.01.008.

Mohammadzadeh Khani, H., Kinnard, C., Lévesque, E., 2022. Historical trends and projections of snow cover over the high Arctic: A review. Water 14 (4), http://dx.doi.org/10.3390/w14040587.

Neudert, M., Arndt, S., Hendricks, S., Hoppmann, M., Schulze, M., Haas, C., 2024. Improved Sub-Ice platelet layer mapping with Multi-Frequency EM induction sounding. J. Appl. Geophys. 230, 105540. http://dx.doi.org/10.1016/j.jappgeo.2024.105540.

Provost, C., Sennéchael, N., Miguet, J., Itkin, P., Rösel, A., Koenig, Z., Villacieros-Robineau, N., Granskog, M.A., 2017. Observations of flooding and snow-ice formation in a thinner Arctic sea-ice regime during the N-ICE2015 campaign: Influence of basal ice melt and storms. J. Geophys. Res.: Ocean. 122 (9), 7115–7134. http://dx.doi.org/10.1002/2016JC012011.

Reid, J.E., Bishop, J., 2004. Post-processing calibration of frequency-domain electromagnetic data for sea-ice thickness measurements. Explor. Geophys. 35 (4), 283–287.

Reid, J., Pfaffling, A., Worby, A., Bishop, J., 2006. In situ measurements of the direct-current conductivity of Antarctic Sea ice: implications for airborne electromagnetic Sounding of Sea-ice thickness. Ann. Glaciol. 44, 217–223. http://dx.doi.org/10.3189/172756406781811772.

Reid, J.E., Worby, A.P., Vrbancich, J., Munro, A.I.S., 2003. Shipborne electromagnetic measurements of Antarctic sea-ice thickness. Geophysics 68 (5), 1537–1546. http://dx.doi.org/10.1190/1.1620627.

Saenz, B.T., Arrigo, K.R., 2012. Simulation of a Sea Ice ecosystem using a hybrid model for slush layer desalination. J. Geophys. Res.: Ocean. 117 (C5), http://dx.doi.org/10.1029/2011JC007544.

SmartICE Sea Ice Monitoring and Information Inc, 2021. Our smart technology. URL: https://smartice.org/our-smart-technology/.

Stroeve, J., Notz, D., 2018. Changing state of Arctic sea ice across all seasons. Environ. Res. Lett. 13 (10), 103001.

Timco, G., Weeks, W., 2010. A review of the engineering properties of sea ice. Cold Reg. Sci. & Technol. 60 (2), 107–129. http://dx.doi.org/10.1016/j.coldregions.2009.10.003.

Vilhelmsen, T.B., Døssing, A., 2022. Drone-towed controlled-source electromagnetic (CSEM) system for near-surface geophysical prospecting: on instrument noise, temperature drift, transmission frequency, and survey set-up. Geosci. Instrum. Methods Data Syst. 11 (2), 435–450. http://dx.doi.org/10.5194/gi-11-435-2022.

Virtanen, P., Gommers, R., Oliphant, T.E., Haberland, M., Reddy, T., Cournapeau, D., Burovski, E., Peterson, P., Weckesser, W., Bright, J., et al., 2020. SciPy 1.0: fundamental algorithms for scientific computing in Python. Nature Methods 17 (3), 261–272. http://dx.doi.org/10.1038/s41592-019-0686-2.

Wait, J.R., 1982. Chapter III - Electromagnetic induction and Loop–Loop Coupling. In: Wait, J.R. (Ed.), Geo-Electromagnetism. Academic Press, pp. 101–139. http://dx.doi.org/10.1016/B978-0-12-730880-7.50007-7.